DAMPING CAPACITY OF A SEALED SQUEEZE FILM BEARING*

M. M. Dede, M. Dogan, and R. Holmes
University of Southampton
Southampton, U. K.

In an earlier paper [1] the advantages of incorporating an open-ended or weakly-sealed squeeze-film bearing in a flexible support structure simulating an aero-engine assembly were examined. In the present paper attention is given to empirically modelling the hydrodynamics of the more usual tightly-sealed squeeze-film bearing, with a view to assessing its damping performance.

INTRODUCTION

A squeeze-film is an annulus of oil supplied between the outer race of a rolling-element bearing (or the bush of a sleeve bearing) and its housing. It is often used as a multi-directional damping element for the control of rotor vibrations.

In most aeroengine applications, the purpose of the squeeze film is to introduce damping so that the rotor can safely negotiate any critical speeds and operate smoothly at a higher speed. The amount of damping can be quite critical: If it is too little, excessive movement will take place within the squeeze-film annulus, if too great the damper will act like a rigid link, making its presence superfluous.

A squeeze-film damper is in effect a journal bearing in which the inner member does not rotate. Hence, it is not possible to assign to it any linear stiffness coefficients which might allow the oil film to take any gravity or other static load, since such coefficients are directly dependent on journal speed. Any lift emanates instead from non-linear effects. For certain operating conditions, such as in the regions of critical speeds, where any static load is small compared to the dynamic load, circular concentric orbits could possibly be assumed, with the result that quasi-linear amplitude-dependent coefficients could be used. Linear analyses could thus be carried out to obtain the vibration orbits in an interative fashion and transmitted forces could be

*The authors gratefully acknowledge Rolls Royce (UK) Limited for their financial support, and ASME for permission to publish.

computed. For cases where the static load is not small a non-linear analysis is called for. Any analysis requires a specification of the effect of cavitation, which has a profound influence on the dynamic load-carrying capacity. Indeed, an uncavitated film may be shown to lead to the complete elimination of load-carrying capacity.

In order to investigate closely the performance of the squeeze-film damper in this kind of application, an experimental rigid rotor [1] was designed and built to simulate an aeroengine gas turbine running at speeds up to 6000 rev/min in rolling-element bearings, one mounted into a housing with an annular gap constituting the squeeze-film damper. This damper was provided with a circumferential groove and supplied with oil at a prescribed pressure. Each land on either side of the groove was of diameter 130 mm and length 9 mm and the radial clearance of the squeeze-film was 0.216 mm. The purpose of the test rig is to study the orbits of vibration and dynamic squeeze-film pressures resulting from various degrees of mass unbalance.

Notation

c	radial clearance of squeeze film
d	seal gap
e	journal eccentricity
$f(\overline{z})$	function of $\overline{z}$
h	squeeze-film thickness
$\overline{h}$	nondimensional film thickness = $h/c = 1 + \varepsilon\cos\theta$
ℓ	radial width of seal
L	bearing-land length
m	effective rotor mass
p	oil film pressure
$p_c(\theta)$	pressure using the long-bearing approximation
p_o	pressure at maximum film thickness
p_s	supply pressure
p_{cav}	cavitation pressure
$\overline{p}$	nondimensional film pressure = $p/\eta\omega(R/c)^2$
$\overline{p_o}$	nondimensional pressure at maximum film thickness = $p_o/\eta\omega(R/c)^2$
$\overline{p_s}$	nondimensional supply pressure = $p_s/\eta\omega(R/c)^2$
$\overline{p_{cav}}$	$p_{cav}/\eta\omega(R/c)^2$
P	static load per land
P_c	dynamic load per land = $mu\omega^2$

P_1, P_2	squeeze-film forces in radial, transverse directions
Q	$P/mc\omega^2$
Q_c	$P_c/mc\omega^2 = u/c$
R	bearing radius
t	time
u	eccentricity of mass unbalance
z	axial coordinate
$\overline{z}$	z/L
α	attitude angle measured in direction of unbalance force rotation
β	nondimensional viscosity = $\eta R(L/c)^3/m\omega$
γ	end leakage flow coefficient
ε	eccentricity ratio = e/c
η	oil viscosity
θ	circumferential coordinate
θ_1, θ_2	oil film boundaries
λ	end-leakage factor = $(c/d)^3 \ell/L$
ω	angular velocity of rotor.

THEORETICAL TREATMENT

The Reynolds equation, suitably adapted for a squeeze-film bearing in which the inner member does not rotate, may be written in a nondimensional form as

$$\frac{\partial}{\partial\theta}\left(\overline{h}^3 \frac{\partial\overline{p}}{\partial\theta}\right) + \left(\frac{R}{L}\right)^2 \frac{\partial}{\partial\overline{z}}\left(\overline{h}^3 \frac{\partial\overline{p}}{\partial\overline{z}}\right) = 12(\varepsilon'\cos\theta + \varepsilon\alpha'\sin\theta) , \quad (1)$$

where $$\overline{p} = p/\eta\omega\left(\frac{R}{c}\right)^2 ,$$

$$\overline{h} = h/c = 1+\varepsilon\cos\theta ,$$

$$\overline{z} = z/L ,$$

and $$(') = d/d(\omega t).$$

The variables are given in the notation.

A common type of squeeze-film damper configuration with a central circumferential oil groove and without end seals was investigated in ref [1]. For such a damper, it was assumed that the oil flow in the circumferential direction was negligible when compared with the flow in the axial direction. This is known as the short-bearing approximation. Hence the first term on the left-hand side of eqn (1) was dropped.

Integrating twice with respect to $\bar{z}$, and putting,

$$\bar{p} = \bar{p}_s \text{ at } \bar{z} = -1/2$$

and

$$\bar{p} = 0 \text{ at } \bar{z} = 1/2,$$

gave

$$\bar{p}(\theta,\bar{z}) = 6(\frac{L}{R})^2 \frac{(\varepsilon'\cos\theta + \varepsilon\alpha'\sin\theta)}{(1 + \varepsilon\cos\theta)^3} (\bar{z}^2 - \frac{1}{4}) + \bar{p}_s (\frac{1}{2} - \bar{z}) \quad (2)$$

This is the general expression for nondimensional pressure in a short squeeze-film with a circumferential oil supply groove and without end seals.

The sealed squeeze-film

It is not uncommon to use seals in squeeze-film dampers to reduce end-leakage and thus to increase the effective damping. This application, however, makes computations difficult to carry out since any mathematical model for predicting the squeeze-film pressure is dependent on the amount of oil leakage allowed by the seals. First, let us consider that the seals allow only small leakage from the ends of the damper. It is therefore assumed that the pressure gradient in the axial direction is negligible compared to that in the circumferential direction. This is known as the long-bearing approximation. Hence eqn.(1) becomes

$$\frac{\partial}{\partial\theta}(\bar{h}^3 \frac{\partial\bar{p}}{\partial\theta}) = 12(\varepsilon'\cos\theta + \varepsilon\alpha'\sin\theta) \quad (3)$$

The solution of eqn (3) for pressure, satisfying boundary conditions $\bar{p} = \bar{p}_o$ at $\theta = 0$, and 2π is readily available in the literature [2] and is quoted here as

$$\bar{p}_c(\theta) = -12\alpha'(\frac{\varepsilon}{2+\varepsilon}) \frac{(2 + \varepsilon\cos\theta)\sin\theta}{(1 + \varepsilon\cos\theta)^2} + 6\frac{\varepsilon'}{\varepsilon}\left[\frac{1}{(1 + \varepsilon\cos\theta)^2} - \frac{1}{(1 + \varepsilon^2)^2}\right] + \bar{p}_o \quad (4)$$

where $\bar{p}_o$ is the nondimensional pressure at the maximum film thickness. It could be taken as the supply pressure $\bar{p}_s$ but more reasonably can be obtained from the short-bearing pressure expression (eqn (2)) by setting the conditions $\bar{p}(\theta,\bar{z}) = \bar{p}_o$ at $\theta = 0$, and averaging over the land length. This gives

$$\bar{p}_o = -(\frac{L}{R})^2 \frac{\varepsilon'}{(1 + \varepsilon)^3} + \bar{p}_s,$$

and ensures that $\bar{p}_c(\theta)$ in eqn (4) is not a function of $\bar{z}$. $\bar{p}_s$ is used instead of $\bar{p}_s/2$ since with sealing there will be little attenuation of p_s. Eqn (4) is true only for squeeze-film bearings in which the pressure gradient in the axial direction is relatively small, or for bearings which have a large length to diameter ratio.

It appears that neither the short-film model nor the long-film model offers a suitable solution from which to calculate the pressure distribution in a centrally-grooved and sealed squeeze-film damper with a restricted but not necessarily small oil leakage. This is because the pressure gradients in both axial and circumferential directions should both be significant for such dampers. For this reason and for speed of computation using non-linear programs, an analytical pressure expression which includes the effect of axial oil flow as well as circumferential oil flow is essential in order to calculate the squeeze-film forces.

To construct such an analytical model, let us assume that the pressure distribution in the $\bar{z}$-direction in a centrally grooved and sealed squeeze-film damper is to be built up as illustrated in Fig.1. Now the boundary condition at $\bar{z} = -1/2$ is readily available as the oil supply pressure in the groove, but the boundary condition at the ends of the squeeze-film (at $\bar{z} = 1/2$) is dependent on the oil-leakage flow rate. For a given damper design this boundary condition may be specified by introducing an end-leakage factor, say λ, and writing the boundary condition as

$$\bar{p} = \lambda \, \bar{p}_c(\theta),$$

in which $\lambda = 0$ for full leakage and $\lambda = 1$ for zero leakage.

$\bar{p}_c(\theta)$ is readily given by eqn (4) as the nondimensional pressure in the θ-direction for the relatively simple case of the long-bearing approximation. It should be noted that this allows pressure to be variable in the circumferential direction at the ends of the damper, whereas often the short-bearing approximation is used in conjunction with the specification of a constant pressure at the ends of the damper.

Now using these boundary conditions as

$$\bar{p} = \bar{p}_s \text{ at } \bar{z} = -1/2$$

and

$$\bar{p} = \lambda \bar{p}_c(\theta) \text{ at } \bar{z} = 1/2,$$

we obtain the final form of the modified pressure expression

$$\bar{p}(\theta,\bar{z}) = 6\left(\frac{L}{R}\right)^2 \frac{(\varepsilon'\cos\theta + \varepsilon\alpha'\sin\theta)}{(1 + \varepsilon\cos\theta)^3} \left(\bar{z}^2 - \frac{1}{4}\right) + \lambda\bar{p}_c(\theta) \left(\bar{z} + \frac{1}{2}\right)$$

$$+ \bar{p}_s\left(\frac{1}{2} - \bar{z}\right) \qquad (5)$$

Fig. 2(a) shows a typical set of circumferential pressure distributions at the mid-land position for two different values of the factor λ, together with the theoretical predictions for the short-bearing and the long-bearing film assumptions. Fig. 2(b) shows a comparison of axial pressure distributions between the short-bearing and the modified film model for $\lambda = 0.09$. The indication is that the modified film model may provide a useful approximation to the experimental case when the value of λ is selected correctly.

Calculation of squeeze-film forces with curtailment of negative pressure

The squeeze-film forces P_1 and P_2 are obtained by integrating the squeeze-film pressure distribution in directions respectively along and normal to the line of centres of the journal and the bearing as follows:

$$P_{1,2} = -\eta\omega\left(\frac{R}{c}\right)^2 RL\int_{\theta_1}^{\theta_2}\int_{-\frac{1}{2}}^{\frac{1}{2}} \overline{p}(\theta,\overline{z}) \begin{pmatrix}\cos\theta \\ \sin\theta\end{pmatrix} d\overline{z}d\theta \qquad (6)$$

where θ_1 and θ_2 are the film boundaries in the circumferential direction.

In this work, with a view to obtaining adequate predictions of vibration orbits, each numerical hydrodynamic pressure distribution was curtailed at its experimentally-observed negative pressure limit before integration to obtain the squeeze-film forces as in ref [1].

Experimental tests

Tests were first carried out using oil of viscosity 6.15 cp, an end-plate clearance of 0.0635 mm and a supply pressure of 5 lbf/in^2 gauge (345 kN/m^2). Fig. 3(a) shows counter-clockwise orbits within the clearance circle of 0.216 mm radius,and dynamic pressure recordings at a mid land position at the base of the damper, at various rotor speeds for $Q_C = 0.459$, while Fig. 3(b) shows the corresponding numerical predictions, for which the value of the λ factor used was 0.09. The negative pressure limit noted in each experimental pressure recording was used as a limiting condition for the corresponding numerical computation of dynamic pressure. Similar comparisons for a higher value of Q_C of 1.055 are given in Figs.4(a) and (b) again using a λ factor of 0.09 for the numerical computations. These results show experimental vibration orbits and pressure waveforms in good agreement with their numerical counterparts. In all the experimental pressure waveforms the horizontal base line denotes atmospheric pressure.

Effect of supply pressure on the damper performance

Since the supply pressure is added linearly to the dynamic

variation in the λ factor appears to be relatively small, in particular for tight sealing, that is low values of d/c.

SOME FURTHER CONSIDERATIONS OF THE OUTLET BOUNDARY CONDITION

As already pointed out the outlet boundary condition for the sealed squeeze-film is dependent on the oil leakage flow rate allowed by the seals. A means of specifying this boundary condition was given by the introduction of an end leakage factor λ. Some further considerations relating to the introduction of this λ factor will now be given.

Assume a solution to the Reynolds equation (eqn 1) of the form

$$\overline{p}(\theta,\overline{z}) = f(\overline{z})\ \overline{p}_c(\theta), \tag{7}$$

where $f(\overline{z})$ and $\overline{p}_c(\theta)$ are functions for pressure in the axial and circumferential directions respectively, the latter being specified at the mid-land position. Substituting eqn (7) into eqn (1) and dividing by $\overline{p}_c(\theta)\overline{h}^3$, gives

$$\overline{b} + g^2\ f(\overline{z}) - \left(\frac{R}{L}\right)^2 \frac{d^2 f}{d\overline{z}^2} = 0 \tag{8}$$

where $\overline{b} = 12\ (\varepsilon' \cos\theta + \varepsilon\alpha' \sin\theta)/\overline{p}_c\ (\theta)\ \overline{h}^3$, and

$$g^2 = \frac{\partial}{\partial\theta}\left(\overline{h}^3 \frac{\partial \overline{p}_c(\theta)}{\partial\theta}\right)/\overline{p}_c(\theta)\ \overline{h}^3 .$$

The solution of eqn (8) for $f(\overline{z})$, with g^2 being treated as a parameter, is straight forward, and is of the form

$$f(\overline{z}) = C_1 e^{gL\overline{z}/R} + C_2 e^{-gL\overline{z}/R} - \frac{\overline{b}}{g^2} \tag{9}$$

where C_1 and C_2 are constants to be determined from the boundary conditions. For the damper under consideration these boundary conditions are:

$$\overline{p}(\theta,\overline{z}) = \overline{p}_s \text{ at } \overline{z} = -1/2,$$

and a boundary condition at $\overline{z} = 1/2$ which can be obtained by considering the axial flow balance across any unit circumferential area around the seal as

$$-\frac{h^3}{12\eta}\left(\frac{\partial p}{\partial z}\right) = \frac{d^3 p}{12\eta\ell},$$

where d is the end seal gap width,
ℓ is the effective length of the gap,

pressure, the effect on the vibration orbits of a higher supply pressure should theoretically be akin to the effect of a lower negative pressure. In fact, an increase in the supply pressure would result in a reduction in the orbit size, and sufficient increase would suppress the negative pressure region completely and thus eliminate the load carrying capability of the squeeze-film [3]. To show the effect of supply pressure on the vibration orbits and cavitation pressure, a set of experimental recordings is given in Fig. 5(a) for Q_c equal to 1.055. Fig. 5(b) shows the corresponding numerical predictions for $\lambda = 0.09$. For these tests supply pressures of 5, 25 and 45 psig (34.5, 172 and 310 kN/m^2) were used. From these figures, it can be seen that the reductions in the orbit size are substantial between 5 and 25 psig , whilst the reductions between 25 and 45 psig are relatively small. An accompanying feature is the development of negative pressure with increase in supply pressure, as can clearly be seen in the recordings of dynamic pressure. This may be due to the fact that for 5 psig, venting from atmosphere takes place, while for higher supply pressures this is prevented by continuous flushing. Such flushing would remove cavitation bubbles and allow the tension spikes to form as shown at the higher supply pressures. It is also interesting to note that no significant rise in the positive peak pressure level was observed or predicted with increase in supply pressure, probably due to the accompanying reduction in orbit size.

Effect of the sealing gap on damper performance

The next phase of the present work was to investigate the effect of end-plate sealing on damper performance and thus to give a graphical estimation for the value of the λ factor for a given end-plate clearance. For convenience testing was first carried out for a supply pressure of 5 psig.(345 kN/m^2). Three different end-plate clearances of 0.114 mm, 0.139 mm and 0.216 mm were used, being set by the insertion of spacing shims. The experimental recordings shown in Fig. 6(a) are for a Q_c value of 0.549, a speed of 3500 rev/min and for an oil vicosity of 6.15 cp. These compare with the display of Fig. 3(a) (3500 rev/min) for a sealing gap of 0.0635 mm. Fig. 6(b) shows the corresponding numerical predictions. For each sealing gap the value of the most appropriate λ factor is given in the figures. From these comparisons, it can be seen that the general size of the orbit increases with increase in the value of end-plate clearance. Good agreement can also be observed between the experimental recordings and the numerical predictions for both orbits and pressure waveforms. From a wide range of results, covering a variety of rotor speeds, supply pressures and unbalance ratios u/c,a plot of the λ factor against the end-clearance ratio (defined as the ratio of end-plate clearance to the damper radial clearance) is shown in Fig. 7. It indicates that for a given end-clearance the appropriate value of the λ factor is increased with increase in oil viscosity. However, given the viscosity range used, the

p and $\partial p/\partial z$ are the pressure and the pressure gradient at the end of the damper ($z = L/2$) respectively.

This boundary condition has been used by Marmol and Vance [5] with some success. Rearranging and writing in nondimensional form, we obtain,

$$\overline{p}(\theta,\overline{z}) = \overline{p} = -\gamma\overline{h}^3 \left(\frac{\partial \overline{p}}{\partial \overline{z}}\right) \text{ at } \overline{z} = 1/2,$$

where $\gamma = (c/d)^3\, \ell/L$, and is introduced as a flow coefficient.

Thus, in terms of the function $f(\overline{z})$, these boundary conditions are:

$$f(\overline{z}) = \overline{p}_s/\overline{p}_c(\theta) \text{ at } \overline{z} = -1/2, \text{ and}$$

$$f(\overline{z}) = -\gamma\overline{h}^3\, df/d\overline{z} \text{ at } \overline{z} = 1/2.$$

Inserting the above boundary conditions into eqn (9) and solving for C_1 and C_2, we obtain

$$C_1 = \left(\frac{\overline{p}_s}{\overline{p}_c(\theta)} + \frac{\overline{b}}{g^2}\right) e^{gL/2R} - C_2 e^{gL/2R}, \tag{10}$$

where

$$C_2 = \frac{\left(\frac{\overline{b}}{g^2}\right) e^{gL/2R} - \left(\frac{\overline{p}_s}{\overline{p}_c(\theta)} + \frac{\overline{b}}{g^2}\right)(1 + \gamma g\overline{h}^3 L/R)\, e^{3gL/2R}}{(1 - \gamma\overline{h}^3 L/R) - (1 + \gamma g\overline{h}^3 L/R)e^{2gL/R}}$$

Equation (9) for the $f(\overline{z})$ function also requires the functional form of g^2. Observing that as $L/R \to \infty$, $df/d\overline{z} \to 0$ and $f \to 1$, then from eqn (8) g^2 becomes

$$g^2 = -\overline{b} = -12\, (\varepsilon'\cos\theta + \varepsilon\alpha'\sin\theta)/\overline{p}_c(\theta)\overline{h}^3 \tag{11}$$

where $\overline{p}_c(\theta)$ is the nondimensional pressure from the long-bearing approximation of the Reynolds equation. Having obtained the required functions the pressure can then be found from eqn (7) as

$$\overline{p}(\theta,\overline{z}) = \overline{p}_c(\theta)\, (C_1\, e^{gL\overline{z}/R} + C_2\, e^{-gL\overline{z}/R} + 1) \tag{12}$$

where g, C_1 and C_2 are calculated from eqns (11) and (10), respectively. Equation (12) is a general pressure expression for any finite-length squeeze-film damper with central circumferential oil supply and end-seals. A similar approach was used by Barrett et al [6] but for an open-ended journal bearing. It was shown to give reliable results.

Some idea of the variation of the pressure distribution with sealing can be obtained from Figs. 8(a), (b), and (c). Fig.8(a) shows a typical set of circumferential pressure distributions at the mid-land position for two extreme values of the flow coefficient γ ($\gamma = 0$ and $\gamma \to \infty$), together with the theoretical predictions based on the short-bearing and the long-bearing film assumptions. In this comparison the modified film model is also included, using a value of the λ factor of 0.09. Fig. 8(b) shows a comparison of axial pressure distributions for these models, whilst Fig. 8(c) shows a comparison of circumferential pressure distributions at the ends of the damper for the finite-length and the modified film models. It should be noted that the value of γ of 27 corresponds to the case of tight sealing for which the value of λ of 0.09 was found by trial to give the best agreement in respect of orbit size and pressure wave form. From Fig. 8(a), it can be seen that even with the full sealing condition ($\gamma \to \infty$) the corresponding peak pressure is considerably smaller than that obtained from the long-bearing approximation. For full leakage ($\gamma = o$), the finite-length solution is nearly identical to the short-bearing solution, as is expected due to the small L/R ratio employed in the test bearing. As far as the specification of the end boundary condition is concerned, similarity (but not equality) can be observed in Fig. 8(c) between the pressure profiles obtained from the two different approaches of using the λ factor of 0.09 and the γ coefficient of 27.

To give a graphic view of the approach, two sets of numerical orbits and pressures are shown in Figs. 9(a) and (b), using respectively values of γ of 27 and ∞ (the full sealing condition). These results should be compared with the experimental recordings of Fig. 3(a) and the numerical predictions of Fig. 3(b). From these comparisons, it can be seen that, even with full-sealing ($\gamma = \infty$)the predicted orbits are considerably larger than the experimental ones and the ones predicted by using the λ factor of 0.09, in particular for the case of 5800 rev/min. A reversal in the position of the sharp "tail" between 3500 and 4000 rev/min was not observed when using the γ coefficient. The numerical pressure waveforms of Figs 9(a) and (b) also do not show good agreement with experiment. These comparisons are typical of the other experimental cases considered. A general observation was that, using the approach of this appendix, the numerical predictions were in poor agreement with the experimental results, in particular for high values of Q_c and at high rotor speeds, with tight sealing.

The λ factor discussed previously may be introduced into the specification of the outlet boundary condition by again considering the end pressure obtained from the flow balance as follows. This pressure has been shown to be,

$$\overline{p(\theta,\overline{z})} = \overline{p} = -\gamma\overline{h}^3 \left(\frac{\partial \overline{p}}{\partial z}\right) \quad \text{at } \overline{z} = 1/2$$

From eqn (7) the pressure gradient is

$$\frac{(\partial \overline{p})}{\partial \overline{z}} = \overline{p}_c(\theta)\left(\frac{\partial f}{\partial \overline{z}}\right).$$

Hence,

$$p = \overline{p}_c(\theta)\left(-\gamma \overline{h}^3 \frac{\partial f}{\partial \overline{z}}\right) \tag{13}$$

Comparing this with the equation,

$$\overline{p} = \lambda \overline{p}_c(\theta), \tag{14}$$

shows that λ replaces

$$\left(-\gamma \overline{h}^3 \frac{\partial f}{\partial \overline{z}}\right).$$

There are two possible reasons why equation (13) does not give satisfactory results. These may be enumerated as follows:

1) The leakage flow through the end seals may not be truly radial. However, even if a screw type of flow is assumed by increasing γ say, we have seen (Fig. 9(b)) that this still does not give adequate agreement with the experimental results, even when $\gamma = \infty$.

2) Equation (13) assumes reverse flow from the seals when the pressure p is negative. However, this does not seem likely since there is no oil reservoir behind the seals, and indeed in the experiments, ingress of air was the more likely occurrence.

Thus, while there is no obvious parametric link between λ and the dimensions of the end seals, the λ approach appears to be one to give adequate predictions of vibration orbit and dynamic squeeze-film pressure. Fig. 7 can then be used to establish an empirical link between parameters.

CONCLUSIONS

The work presented in this paper has dealt with the performance of the sealed squeeze-film damper when used in aero-engine applications. In such applications, the operation of the damper is governed by five nondimensional groups. These groups are the nondimensional static force Q, the nondimensional dynamic force Q_C, the nondimensional viscosity β, the nondimensional supply pressure $\overline{p}_s$ and the nondimensional cavitation pressure p_{cav}. Good agreement has been observed between experimental observations and numerical predictions using an empirical leakage factor, over a wide range of operating parameters. This work has also demonstrated experimentally that sustained lift of the rotor in the squeeze

film annulus can be obtained without the use of any parallel support stiffness, and the squeeze-film was shown to provide this lift by the assumption of a cavitated film model.

It has been shown that the use of an end-leakage factor λ has resulted in successful predictions of vibration orbits and dynamic pressures in the sealed squeeze-film. It has been demonstrated experimentally that the damping can be increased effectively by decreasing the sealing gap and a means of determining λ for a given gap has been given graphically. One indication was that this gap should be made less than half the damper radial clearance to achieve effective damping.

There remains the problem of needing to know in advance the value of negative pressure to adopt for curtailing the squeeze-film pressure during computation of the squeeze-film forces and orbits in any given application. Experimental recordings of dynamic pressure show that this negative pressure appears to take one of three approximate values:

(i) Approximately atmospheric, when the supply pressure is not great enough to prevent ingress of atmospheric air, which fills the cavitation zone;

(ii) Approximately absolute zero, when cavitation bubbles exist due to the liberation of dissolved gases and fluid vapour. The supply pressure here has to be somewhat higher to prevent ingress of air, but is still not high enough to flush the bubbles away;

(iii) Lower than absolute zero, when the oil temporarily supports tension, many cavitation bubbles in the previous cycles being flushed away by a fairly high supply pressure.

For the bearing assembly considered in this work, when used under most engine conditions, it could reasonably be expected that much of the performance could be such as to produce cavitation pressures in the third region when a value of about -40 psig seems a fair average. This is based on the assumption that the external oil pressure at the squeeze-film groove is likely to be around 40 - 50 psig. It is suggested that, given the highly complicated mechanism of negative pressure development in the squeeze-film, reliance can be placed on the use of fairly high supply pressures to ensure a measure of consistency in the negative pressure at which film rupture is assumed to occur.

REFERENCES

[1] Holmes,R. and Dogan, M. 'Investigation of squeeze film dampers in flexible support structures', NASA Conference Publication 2250 entitled 'Rotor dynamic instability problems in High Performance Turbomachinery - 1982'.

[2] Pinkus, O. and Sternlicht, B. 'Theory of hydrodynamic lubrication'. McGraw-Hill Inc., New York, 1961.

[3] Holmes, R. 'The non-linear performance of squeeze-film bearings'. Jnl Mech.Eng.Sci., Vol.14, no.1, 1972.

[4] Holmes, R. and Dede, M. 'Dynamic pressure determination in a squeeze-film damper'. Inst. Mech.Engrs. Second Int. Conf. on Vibrations in Rotating Machinery, Sept. 1980.

[5] Marmol, R.A. and Vance, J.M. 'Squeeze-film damper charactersitics for gas turbine engines'. ASME Paper No. 77-DET-18, Oct. 1977.

[6] Barrett, L,E,, Allaire, P.E. and Gunter, E.J. 'A finite length correction factor for short bearing theory'. Trans. ASME Jnl Lub. Tech. Vol.102, July 1980.

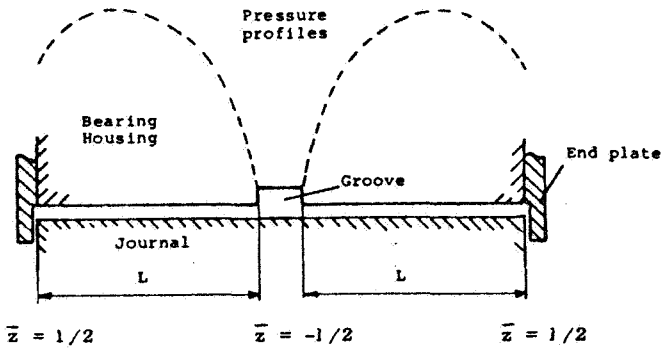

Fig. 1 Damper configuration with circumferential oil supply groove and end plates

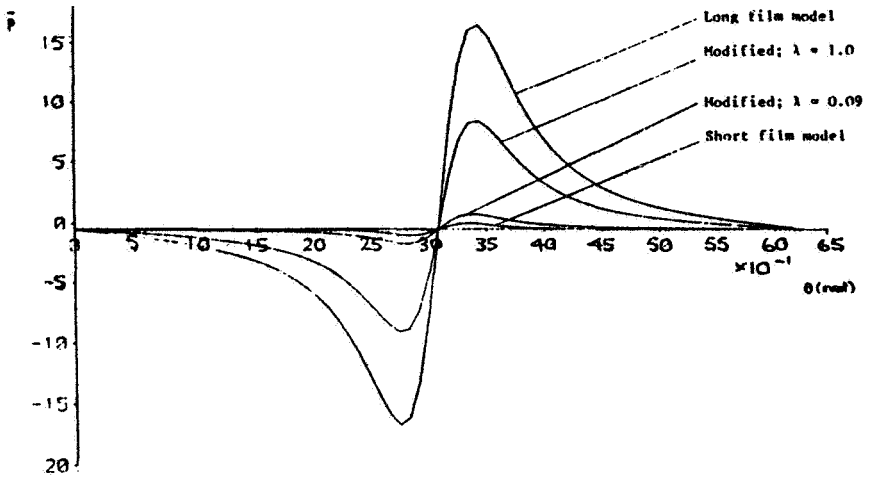

Fig. 2(a) Circumferential pressure distributions

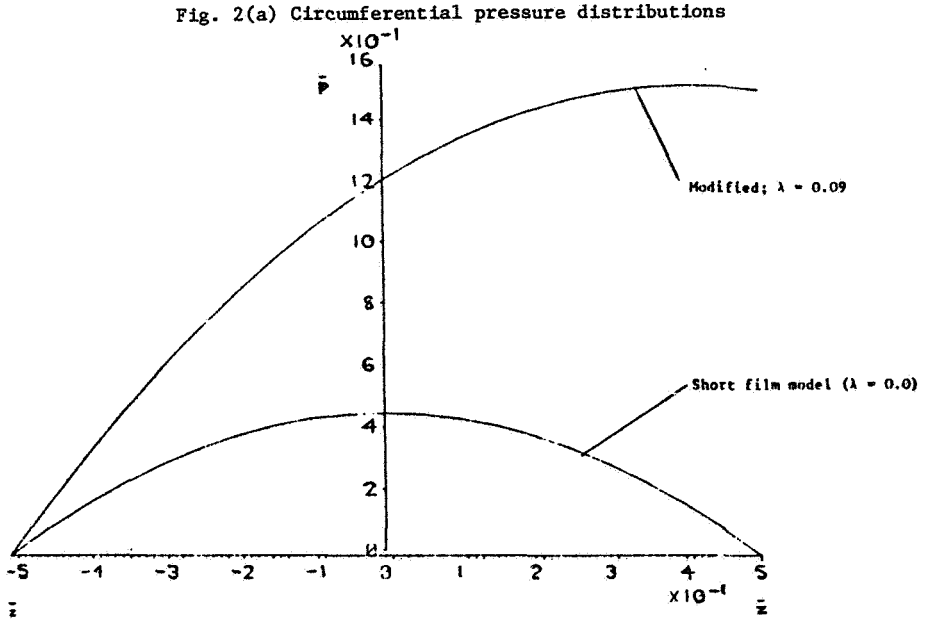

Fig. 2(b) Axial pressure distributions

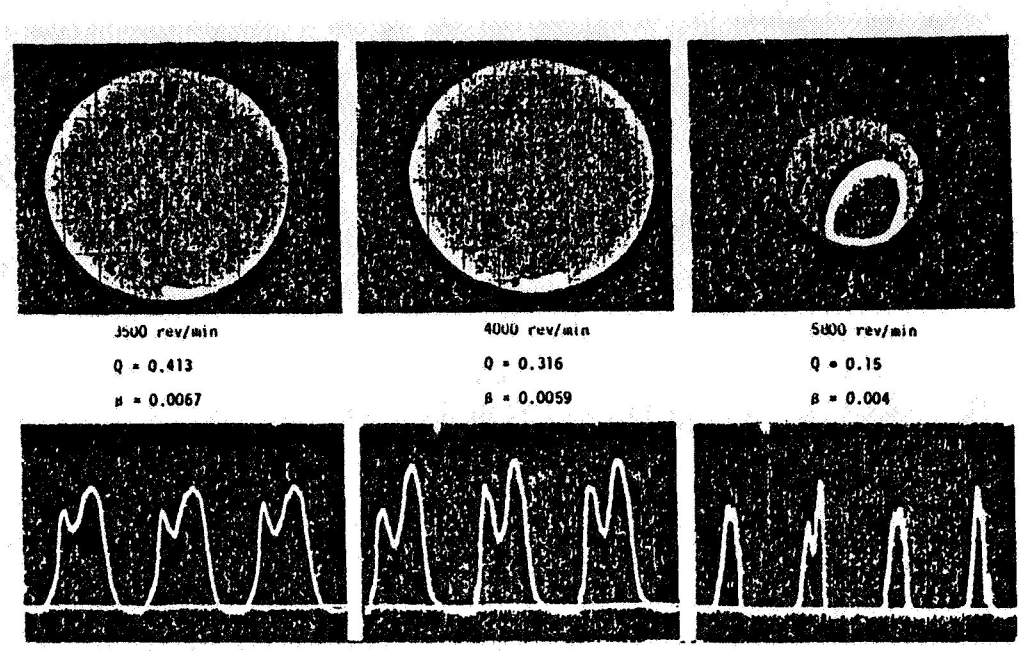

(a)

Vertical Scale

500 psi
3450 kN/m^2

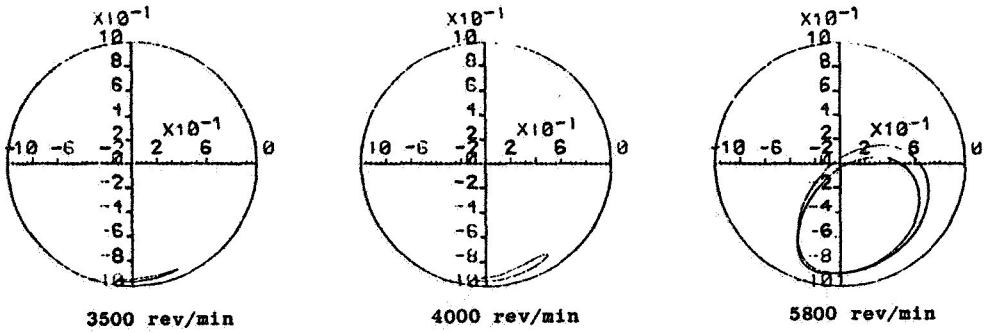

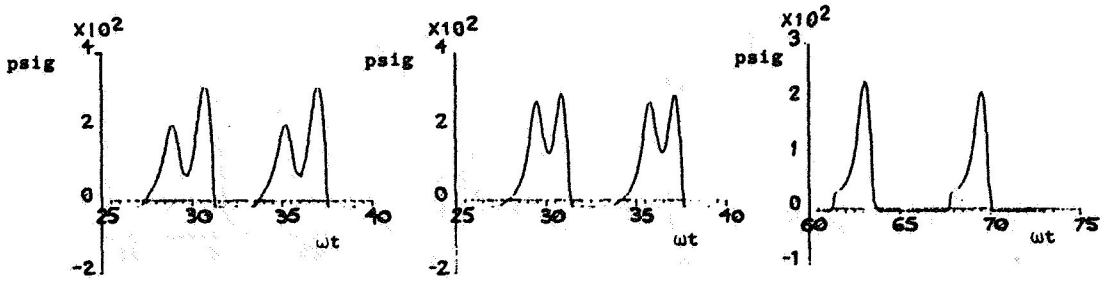

(b)

Fig.3. Q_c = 0.459; (a) experimental orbits and pressure recordings, (b) numerical orbits and pressures.

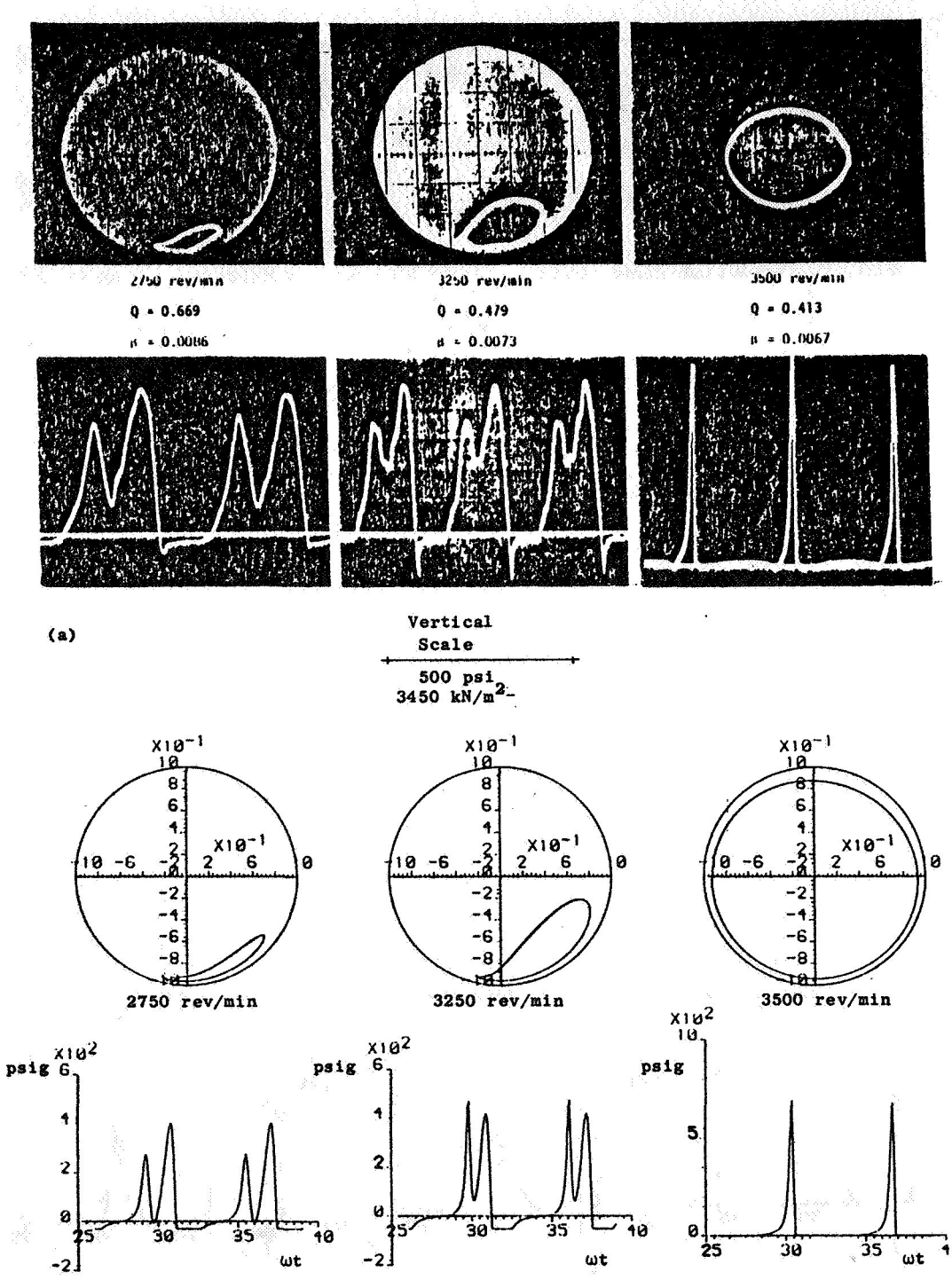

Fig.4 Q_c = 1.055; (a) experimental orbits and pressure recordings, (b) numerical orbits and pressures.

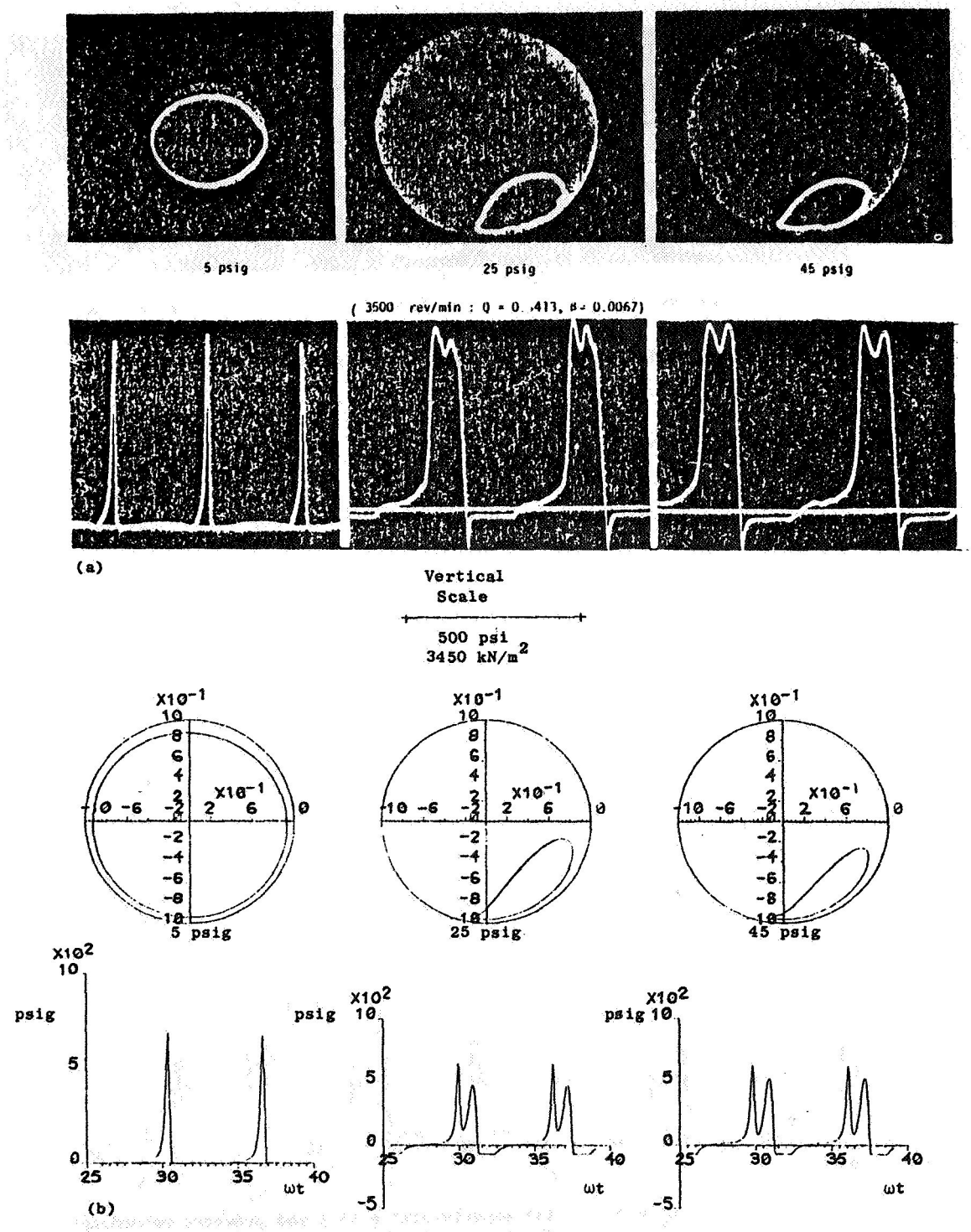

Fig. 5 Q_c = 1.055; (a) experimental orbits and pressure recordings
(b) numerical orbits and pressures

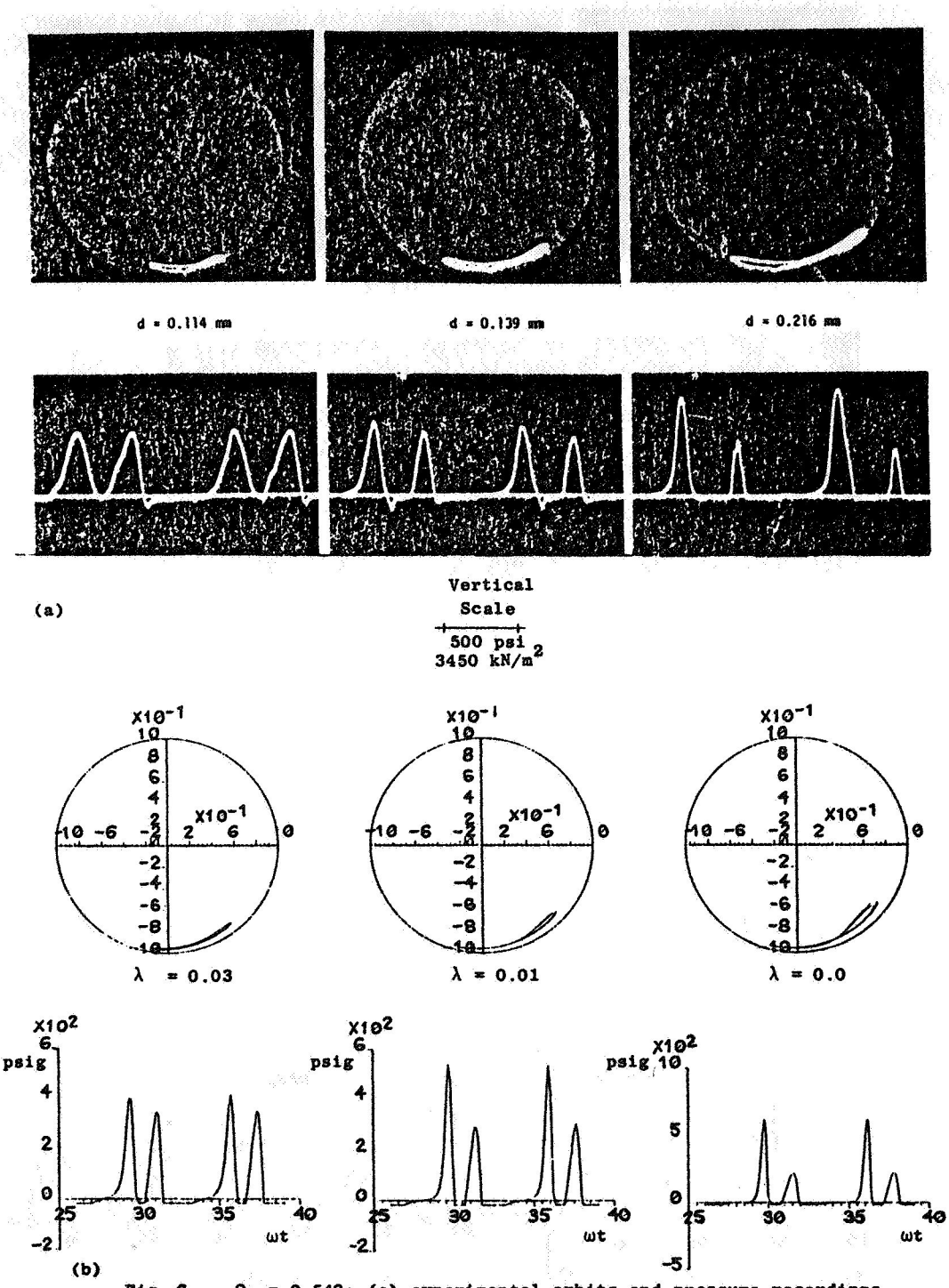

Fig. 6 . Q_c = 0.549; (a) experimental orbits and pressure recordings, (b) numerical orbits and pressures.

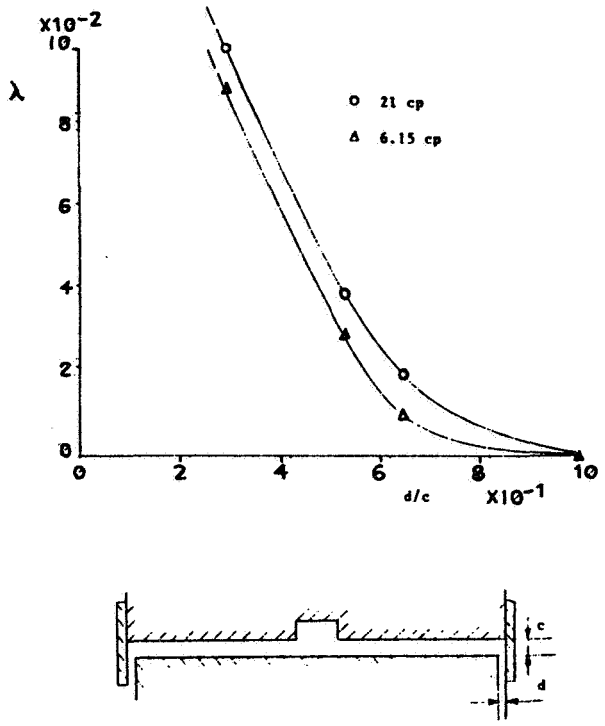

Fig. 7 End-plate seal factor λ vs end-clearance ratio d/c.

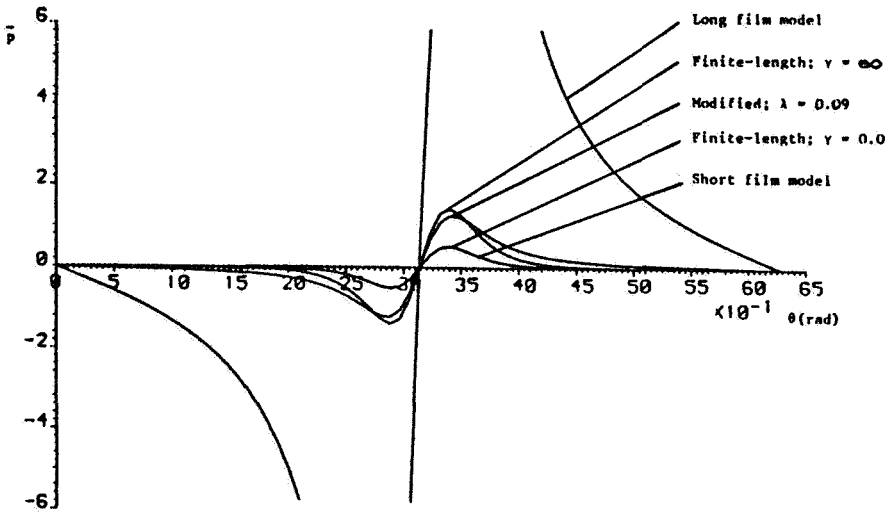

Fig. 8 (a) Circumferential pressure distributions

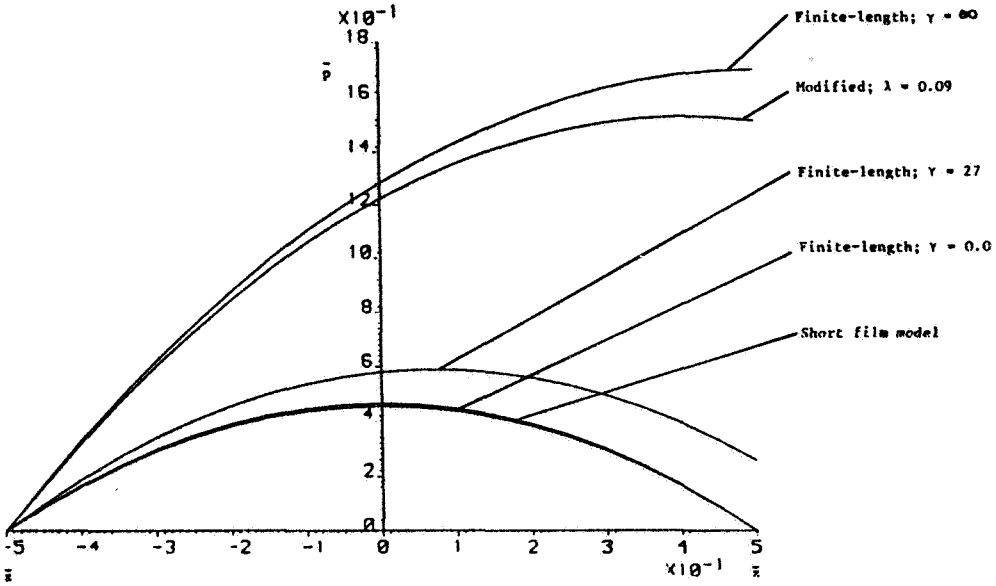

Fig. 8 (b) Axial pressure distributions.

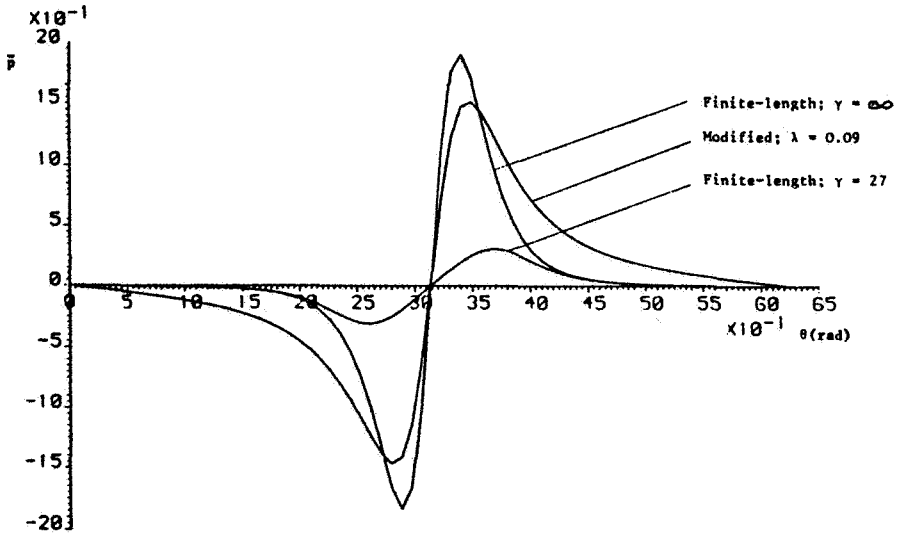

Fig. 8(c) A comparison of circumferential pressures around the seal (at $\bar{z} = 1/2$).

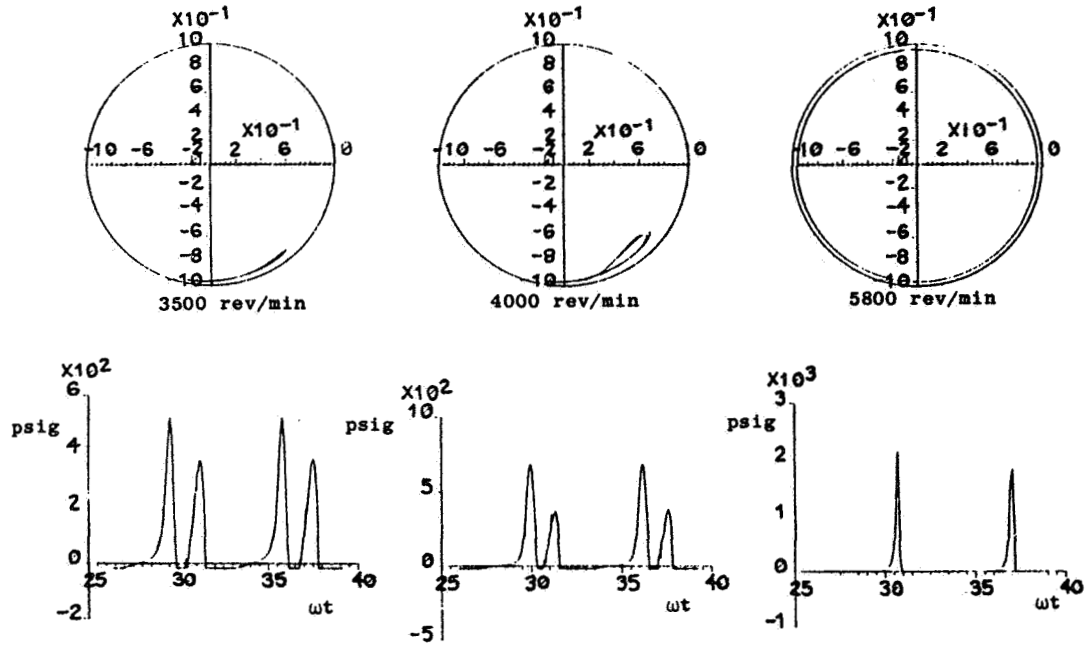

Fig. 9(a). Q_c = 0.459; numerical orbits and pressures using γ = 27

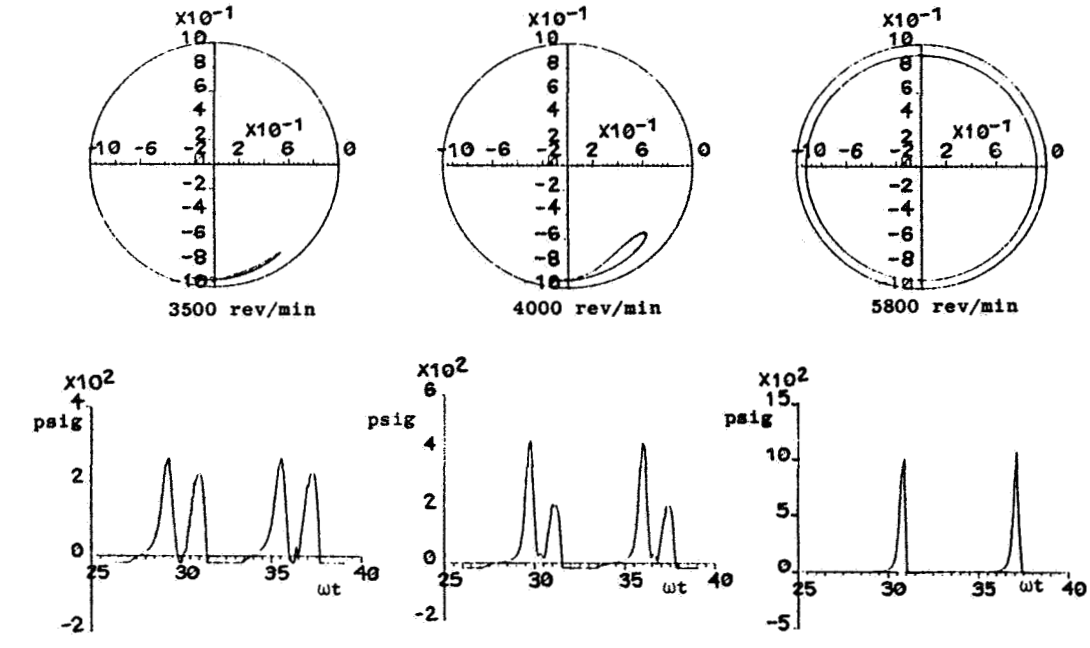

Fig. 9 (b). Q_c = 0.459; numerical orbits and pressures using $\gamma = \infty$.